Time-Reversal Based Range Extension Technique for Ultra-wideband (UWB) Sensors and Applications in Tactical Communications and Networking

Technical Report (Quarterly)

to

Prepared by

Robert C. Qiu

(Principal Investigator)

together with

(Contributing Researchers at Wireless Networking Systems Lab)

Nan (Terry) Guo
Yu Song
Peng (Peter) Zhang
Zhen (Edward) Hu

April 16, 2009

Department of Electrical and Computer Engineering

Center for Manufacturing Research

Tennessee Technological University
Cookeville, TN 38505

20090702327

REPORT DOCUMENTATION PAGE

1. REPORT DATE (DD-MM-YYYY)	2. REPORT TYPE	3. DATES COVERED (From - To)
16-04-2009	Technical Report (Quarterly)	January 16, 2009---April 16, 2009

4. TITLE AND SUBTITLE

Time-Reversal Based Range Extension Technique for Ultra-wideband (UWB) Sensors and Applications in Tactical Communications and Networking

5a. CONTRACT NUMBER

5b. GRANT NUMBER

N00014-07-1-0529

5c. PROGRAM ELEMENT NUMBER

6. AUTHOR(S)

Qiu, Robert C.; Guo, Nan; Song, Yu; Zhang, Peng; Hu, Zhen

5d. PROJECT NUMBER

5e. TASK NUMBER

5f. WORK UNIT NUMBER

7. PERFORMING ORGANIZATION NAME(S) AND ADDRESS(ES)

Tennessee Technological University
115 W. 10th Street
Cookeville, TN 38501

8. PERFORMING ORGANIZATION REPORT NUMBER

9. SPONSORING/MONITORING AGENCY NAME(S) AND ADDRESS(ES)

US Office of Naval Research
875 North Randolph Street
Arlington, VA 22203-1995

10. SPONSOR/MONITOR'S ACRONYM(S)

ONR

11. SPONSOR/MONITOR'S REPORT NUMBER(S)

07PR05074-00

12. DISTRIBUTION/AVAILABILITY STATEMENT

release for public distribution.

13. SUPPLEMENTARY NOTES

14. ABSTRACT

The focus of this report is on major improvement and system test. Receiver sensitivity has been significantly improved and about 3 dB time reversal precoding gain has been observed based on system trial in indoor non-line-ofsight scenario. Theoretical study shows that additional gain can be achieved by using optimum waveform design.
Listed below are major achievements during the quarter:
• multiple integration window sizes;
• comprehensive system test;
• improved receiver sensitivity to -81 dBm;
• 3 to 4 dB time reversal precoding gain in indoor non-line-of-sight scenario.
We will continue to improve the system and conduct more measurements, while seeking some technology transfer opportunities.

15. SUBJECT TERMS

UWB, testbed, time reversal, range extension, sensors, multi-GHz wideband, cognitive radio

16. SECURITY CLASSIFICATION OF:			17. LIMITATION OF ABSTRACT	18. NUMBER OF PAGES	19a. NAME OF RESPONSIBLE PERSON
a. REPORT	b. ABSTRACT	c. THIS PAGE			Francis Otuonye
U	U	U	UU	24	19b. TELEPHONE NUMBER (Include area code) 931-372-3374

REPORT OF INVENTIONS AND SUBCONTRACTS
(Pursuant to "Patent Rights" Contract Clause) (See Instructions on back)

The public reporting burden for this collection of information is estimated to average 1 hour per response, including the time for reviewing instructions, searching existing data sources, gathering and maintaining the data needed, and completing and reviewing the collection of information. Send comments regarding this burden estimate or any other aspect of this collection of information, including suggestions for reducing the burden, to the Department of Defense, Executive Services Directorate (9000-0095). Respondents should be aware that notwithstanding any other provision of law, no person shall be subject to any penalty for failing to comply with a collection of information if it does not display a currently valid OMB control number.

PLEASE DO NOT RETURN YOUR COMPLETED FORM TO THE ABOVE ORGANIZATION. RETURN COMPLETED FORM TO THE CONTRACTING OFFICER.

1.a. NAME OF CONTRACTOR/SUBCONTRACTOR	2.a. NAME OF GOVERNMENT PRIME CONTRACTOR	c. CONTRACT NUMBER	3. TYPE OF REPORT *(X one)*	
Tennessee Technological University	US Office of Naval Research	N00014-07-1-0529	X a. INTERIM	b. FINAL

b. ADDRESS *(Include ZIP Code)*	c. CONTRACT NUMBER	d. AWARD DATE *(YYYYMMDD)*	b. ADDRESS *(Include ZIP Code)*	d. AWARD DATE *(YYYYMMDD)*	4. REPORTING PERIOD *(YYYYMMDD)*
115 W. 10th Street	N00014-07-1-0529	20070116	875 North Randolph Street	20070116	a. FROM 20090116
Cookeville, TN 38501			Arlington, VA 22203-1995		b. TO 20090416

SECTION I - SUBJECT INVENTIONS

5. "SUBJECT INVENTIONS" REQUIRED TO BE REPORTED BY CONTRACTOR/SUBCONTRACTOR *(If "None," so state)*

NAME(S) OF INVENTOR(S) *(Last, First, Middle Initial)* a.	TITLE OF INVENTION(S) b.	DISCLOSURE NUMBER, PATENT APPLICATION SERIAL NUMBER OR PATENT NUMBER c.	ELECTION TO FILE PATENT APPLICATIONS *(X)*				CONFIRMATORY INSTRUMENT OR ASSIGNMENT FORWARDED TO CONTRACTING OFFICER *(X)* e.	
			(1) UNITED STATES		(2) FOREIGN			
			(a) YES	(b) NO	(a) YES	(b) NO	(a) YES	(b) NO
None								

f. EMPLOYER OF INVENTOR(S) NOT EMPLOYED BY CONTRACTOR/SUBCONTRACTOR

(2)(a) NAME OF INVENTOR *(Last, First, Middle Initial)*	g. ELECTED FOREIGN COUNTRIES IN WHICH A PATENT APPLICATION WILL BE FILED	
	(1) TITLE OF INVENTION	(2) FOREIGN COUNTRIES OF PATENT APPLICATION
(b) NAME OF EMPLOYER		
(c) ADDRESS OF EMPLOYER *(Include ZIP Code)*		

SECTION II - SUBCONTRACTS *(Containing a "Patent Rights" clause)*

6. SUBCONTRACTS AWARDED BY CONTRACTOR/SUBCONTRACTOR *(If "None," so state)*

NAME OF SUBCONTRACTOR(S) a.	ADDRESS *(Include ZIP Code)* b.	SUBCONTRACT NUMBER(S) c.	FAR "PATENT RIGHTS" d.		DESCRIPTION OF WORK TO BE PERFORMED UNDER SUBCONTRACT(S) e.	SUBCONTRACT DATES *(YYYYMMDD)* f.	
			(1) CLAUSE NUMBER	(2) DATE *(YYYYMM)*		(1) AWARD	(2) ESTIMATED COMPLETION
None							

SECTION III - CERTIFICATION

7. CERTIFICATION OF REPORT BY CONTRACTOR/SUBCONTRACTOR *(Not required if: (X as appropriate))*   SMALL BUSINESS or   NONPROFIT ORGANIZATION

I certify that the reporting party has procedures for prompt identification and timely disclosure of "Subject Inventions," that such procedures have been followed and that all "Subject Inventions" have been reported.

a. NAME OF AUTHORIZED CONTRACTOR/SUBCONTRACTOR OFFICIAL *(Last, First, Middle Initial)*	b. TITLE	c. SIGNATURE	d. DATE SIGNED
Otuonye, Francis	Associate Vice President	N/A	

DD FORM 882, JUL 2005   PREVIOUS EDITION IS OBSOLETE.

2

Acknowledgment

Executive Summary

The focus of this report is on major improvement and system test. Receiver sensitivity has been significantly improved and about 3 dB time reversal precoding gain has been observed based on system trial in indoor non-line-of-sight scenario. Theoretical study shows that additional gain can be achieved by using optimum waveform design. Listed below are major achievements during the quarter:

- multiple integration window sizes;

- comprehensive system test;

- improved receiver sensitivity to -81 dBm;

- 3 to 4 dB time reversal precoding gain in indoor non-line-of-sight scenario.

We will continue to improve the system and conduct more measurements, while seeking some technology transfer opportunities.

4

Contents

Part I

Testbed Development

Chapter 1

Major Improvements

Our major development work in the last quarter is to test and modify the system. The most significant part is the synchronization at the receiver side.

1.1 Synchronization Improvements

For a burst mode radio system, the synchronization has always been a challenge. In order to make the synchronization more robust for the test-bed, we have made some improvements, which include modification of the frame structure, average samples for start pattern searching and various thresholds adjustment.

1.1.1 Synchronization Review

Before talking about these synchronization improvements, let's first review the receiver's implementation structure and data flow. The functional diagram is shown as Fig. 1.1. The main modules include data interface between FPGA and ADC, integration, synchronization, decision, a finite state machine and thresholds control. Among them, the challenges at the receiver are mainly on the high speed interface, fast integration and the robust synchronization. We are currently using a 3 stage synchronization technique which is shown in Fig. 1.3.
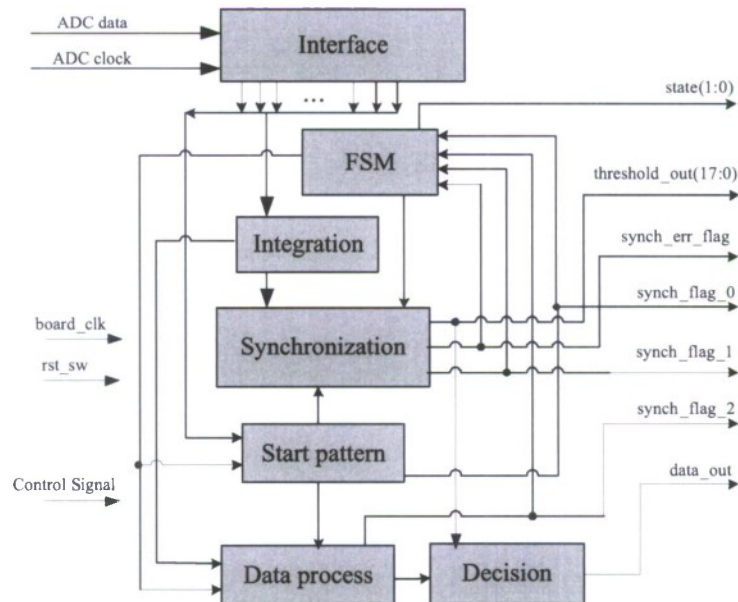
Figure 1.1: Receiver functional diagram

Fig. 1.2 is the data flow for the receiver. First the interface module converts the high speed ADC output data to relatively low speed data streams through several steps. Then the data streams go to start pattern searching module to find the time of arrival and go to integration module for chip level energy integration. There are 32 fast integrators for integration, which are implemented by DSP cores embedded in Virtex-5 FPGA. The synchronization module combines the time of arrival signal and the integration results by finding the integrator with maximum energy, then

it gets the chip threshold. After that the receiver applies frame level synchronization to find the fine timing and make decisions. The finite state machine and variable thresholds control module coordinate all the processes.

Figure 1.2: Receiver data flow

1.1.2 Frame Structure

The system is supposed to find the window with maximum energy in every 40 ns, which is the chip period. Fig. 1.3 shows the new frame structure of the system. The first stage is to search the time of arrival; the second stage is to average 128 chips energy to find the chip threshold; the third stage is to synchronize the whole fra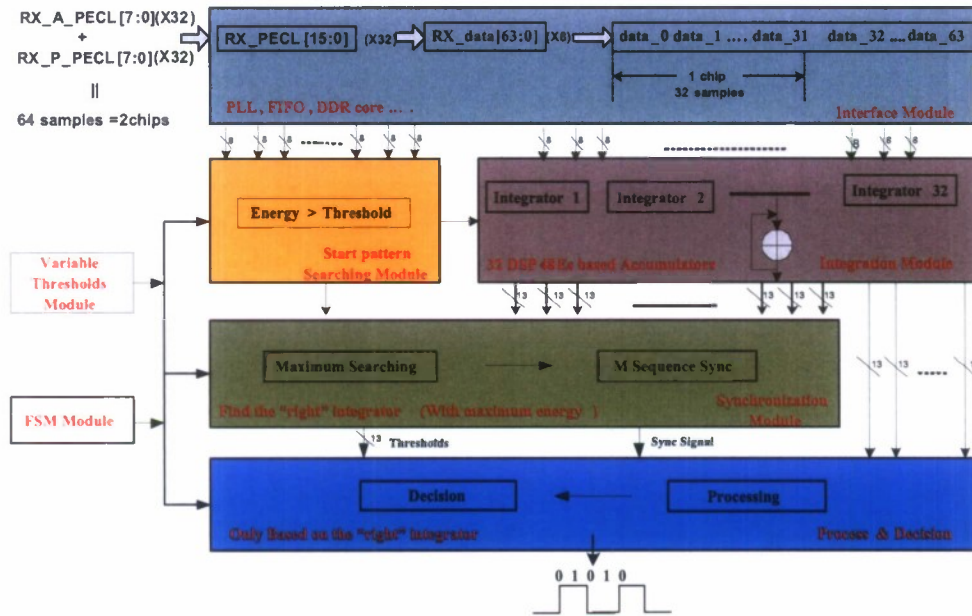me. Data demodulation is performed after the three-stage synchronization. Fig. 1.3 also shows the sliding window integration diagram and the state transition diagram.

The modification in the synchronization head does not change the overall frame structure. The following parameters are kept: system's frame length: 4096 chips or 163.84 μs; payload efficiency: 94.49%; chip sync accuracy: one sample (1.25 ns); and frame sync accuracy: one chip (40 ns). If the overall clock accuracy is 20 PPM, then the maximum time drift is $163.84 \times 10^{-6} = 3.276$ μs.

1.1.3 Dense Pulses

However, even though we averaged the start pattern searching, wc observed that the synchronization error still mainly comes from the first stage. In this stage, the threshold is very sensitive to noise level and DC offset of ADC sampling, especially for longer distance transmission. So we try to send 5 chips long dense pulses at the beginning of each frame to make sure the time of arrival is found each frame since the average value of these chips should be much higher than ordinary ones. Fig. 1.4 shows the real picture of dense pulses at the beginning of each frame.
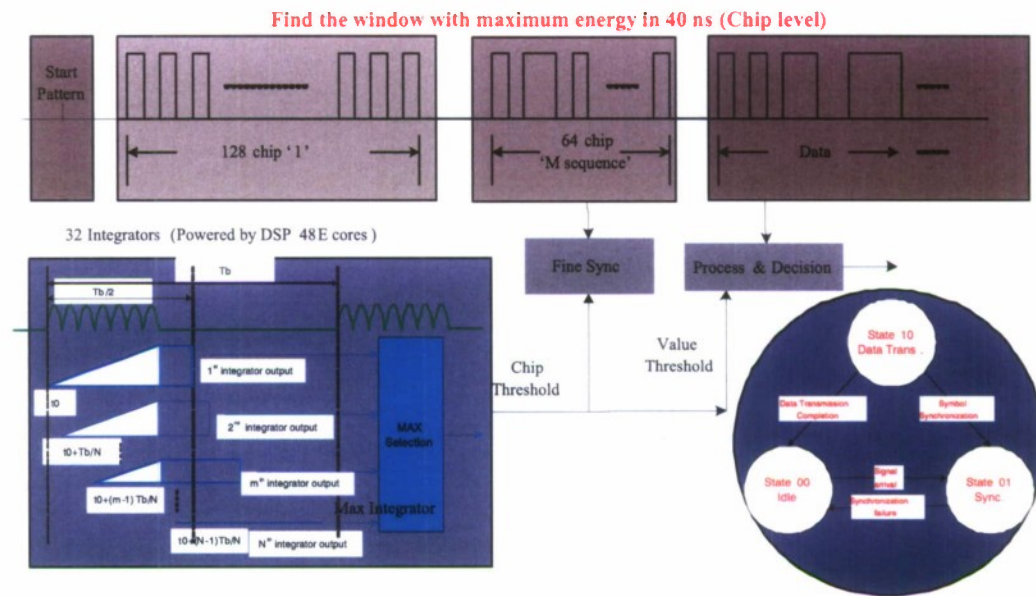
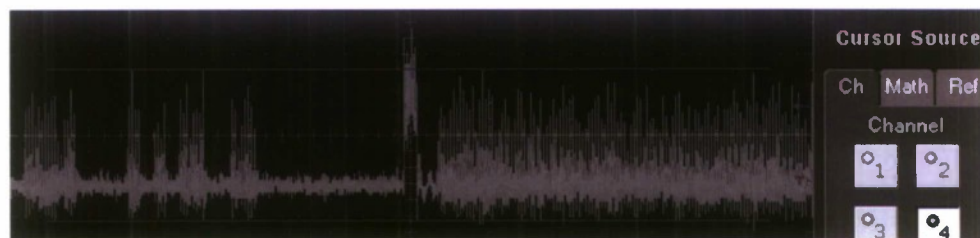Figure 1.3: The new frame structure design

Figure 1.4: The picture of dense pulse at the beginning of each frame

1.1.4 Start Pattern Averaging

For the first synchronization stage, we accumulate the values of 32 consecutive samples and compare it with a threshold to claim whether it is one frame's time of arrival. However, due to the interference and environment's uncertainty, the first stage result should not be so reliable when it just counts on the value only one chip time, because the time frame is too short. So we try to average two chip time samples result to get the averaged value, and compare it with a threshold, Fig. 1.5 shows the diagram of this improvement, where we set a more strict condition to claim the time of arrival result by comparing 5 times(or other number) instead of only one, and is in 5 chips time(or other number), 3 high results are needed to claim the first stage synchronization result. After that, because we send dense pulses at the beginning of each frame and there is a interval between the pulses and the real chips, we delay two chips time before the beginning of second stage.

1.1.5 Other modifications

For the third stage,we also utilized 60 bits M sequence instead of 60 bits OOC code for frame synchronization. This is mainly because the randomness of M sequence is much better than OOC code.

For time reversal system and non time reversal system, the received pulses are very different at the width, typically 6 ns for time reversal and 15 ns for non time reversal. So in the energy integration module, the window size for integration should be different for different signal scenarios. This parameter is to be adjusted in integration module, as described in the last quarter report.

1.2 Threshold Adjustment

For energy detection based receiver, it is well known that the performance depends significantly on the choice of threshold level. A good threshold can be determined by using some channel quality indicator and feedback information provided by the digital processor (back-end) at the receiver. There is an optimum threshold for lowest error rate. To deal with ISI situation, it is proposed to set a threshold based on two worst signal cases.

One phenomenon discovered is that a mono-bit ADC along with proper thresholding can be applied for quantizing the pre-filters coefficients, and the resulting signal still gets focused. It enables the development of a unique time reversal system with much lower complexity. Major points include: (1) optimization of the threshold for quantization; (2) development of an adaptive threshold method; (3) impact of tap spacing and length of the pre-filter. In our case, there are 4 variable thresholds at the receiver side with each corresponds to different stages of synchronization and detection. They are the threshold for start pattern searching, the threshold for ADC bias shift, the code distance for frame level synchronization and the threshold of chip threshold determine at the second synchronization stage. All these values are adjusted by the pushbuttons on the receiver Virtex-5 board and the led lights can show any threshold's adjustment level.

DC offset causes performance degradation in signal processing systems especially for high-speed applications. For our ADC board in the receiver side, the DC shift makes the true quantization value hard to determine, thus makes the threshold vulnerable, especially for the energy detection based receiver with OOK modulation. DC offset can be reduced in real-time by subtracting the mean amplitude from each sample, or by calibrating the ADC board.
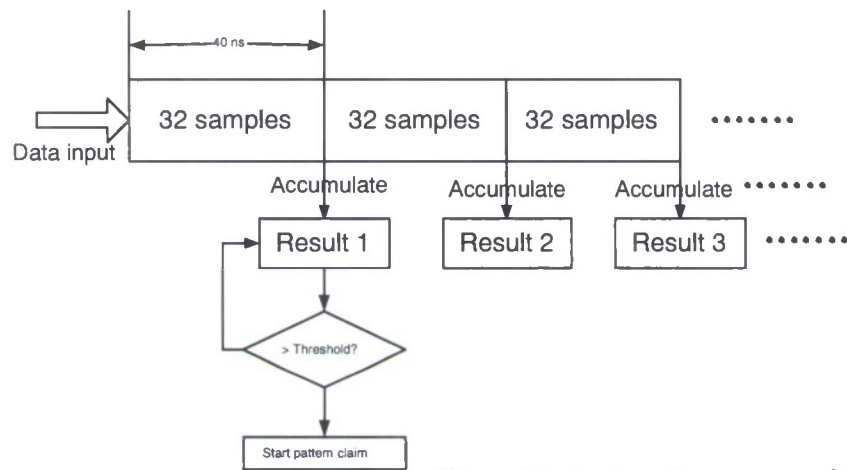
The old start pattern searching
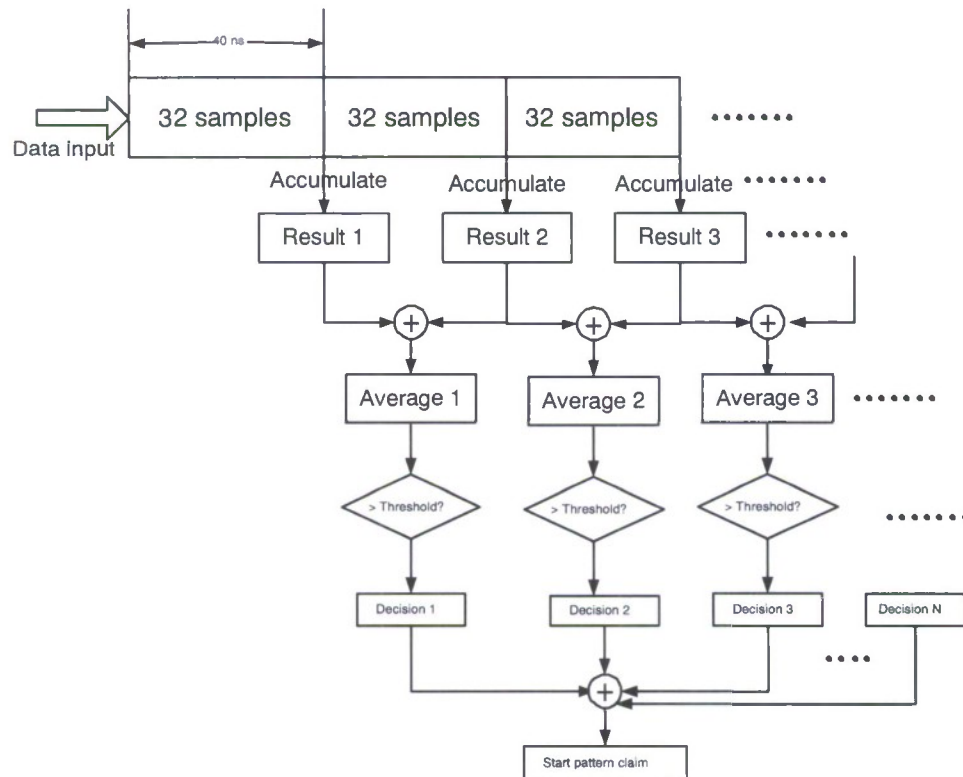
The new start pattern searching

Figure 1.5: Start pattern searching improvement

Chapter 2

FPGA Implementation

2.1   FPGA Timing Closure Issues

For FPGA implementation, meeting timing requirements in spced-critical designs has been always a challenge, and this is often an iterative process ensuring that each and every path in the design meets the required timing. Meeting timing closure is easy and automatic for relatively slow or small designs. However, most designs do not fall into that happy category and as each critical path is adjusted in order to meet timing, new ones are uncovered or created anew. In the case of FPGAs implemented at the 65nm technology node, for example, wire delays can account for 80-to-90% of each path's delay.

An important technique for achieving successful timing closure on an aggressive design is to carefully review the most critical timing constraints. In our case, there are two critical paths at the transmitter: one is from the data loading module to the waveform generator module where huge parallel data steams exist, another critical path is in the parallel to serial conversion module requiring high clock rate. At the receiver side, the most critical path is from the integration module to the synchronization module which performs fast timing aequisition in parallel manner. Achieving clock-to-clock (global) timing for all internal signals in a synchronous design may be easy, but this simple approach will usually overconstrain the design and eventually lead to a failure. Therefore, we have applied different constraints to different paths depending on their timing requirements.

The impact of timing constraints can be seen in Fig. 2.1, where the left picture shows the output waveform from the DAC when appropriate timing constraints are applied, while the right one shows the waveform with unwanted spikes when timing constraints are not properly added.
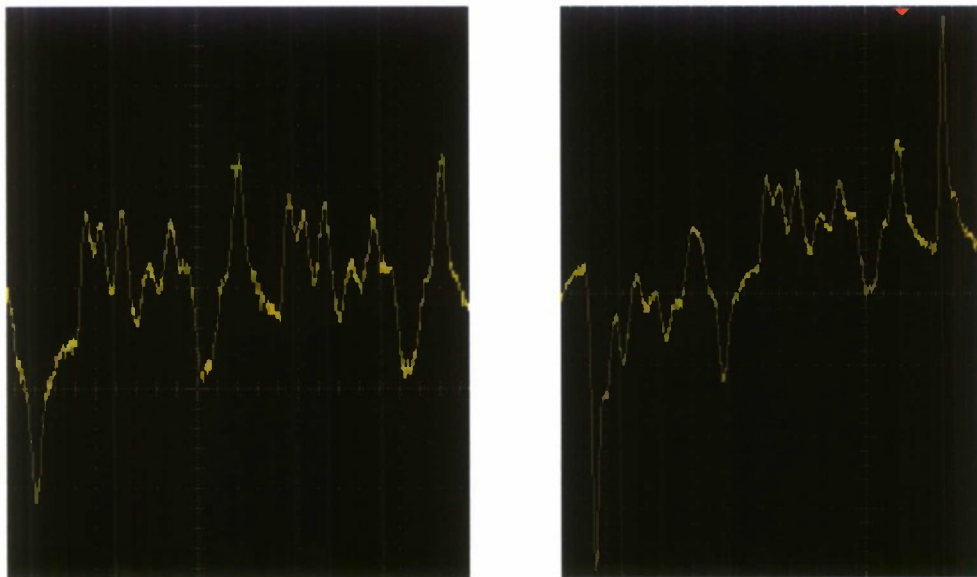
Figure 2.1: Output waveforms comparison with and without applying proper timing constraints

2.2 Major FPGA Implementation Reports

Table 2.1 shows the resource usage for the test-bed back-ends implemented on Xilinx Virtex-5 LXT FPGAs. Note that the FPGA chips used at the transmitter and receiver are of the same model, but the transmitter FPGA chip has 1136 I/O ports while the receiver FPGA chip has only 665 I/O ports. As we can see, at both the transmitter and receiver there are a lot of FPGA resources available. The routing result is shown in Fig. 2.2, and the resource usages are visually displayed.

Transmitter   Receiver
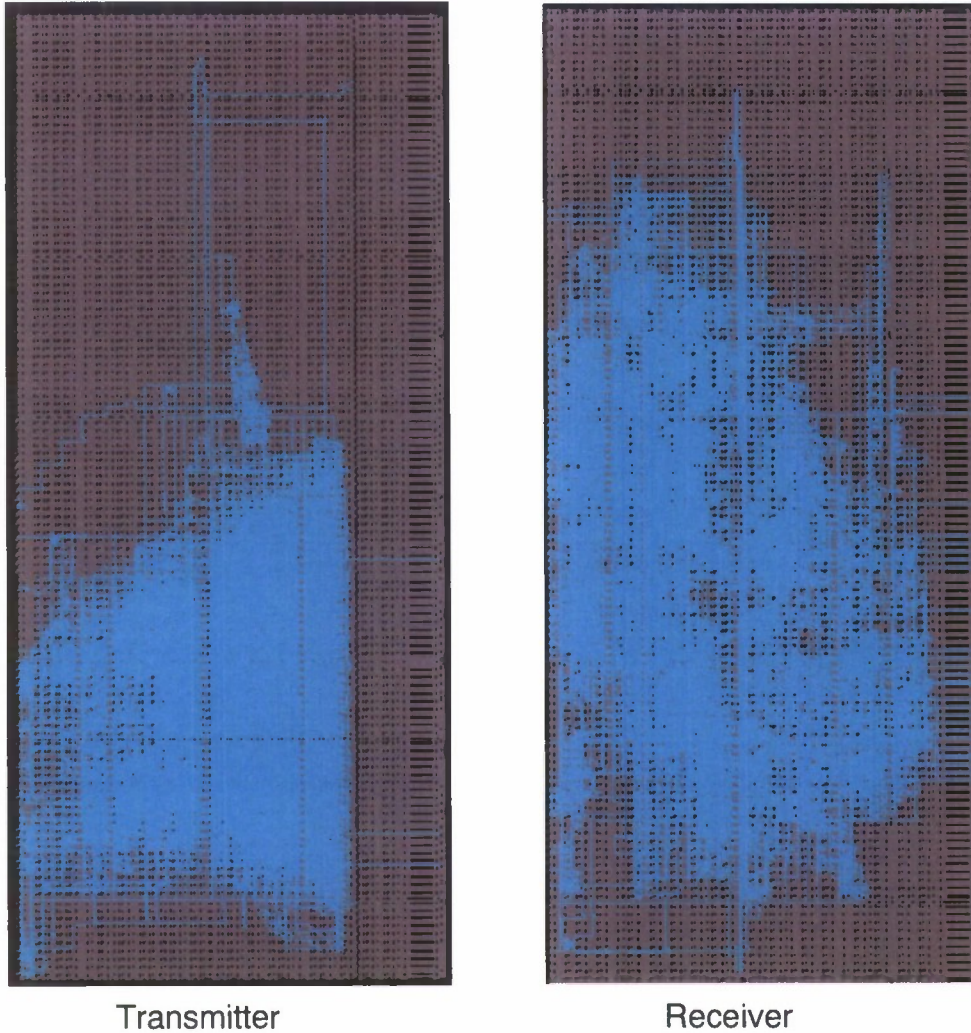
Figure 2.2: FPGA routing results for both transmitter and receiver

Table 2.1: FPGA Implementation statistics at transmitter and receiver

Resources	Transmitter Amount used	Transmitter Percent used	Receiver Amount used	Receiver Percent used
Number of Slice Registers	5314	18%	4184	14%
Number of Slice LUTs	5019	13%	3088	10%
Number of occupied Slices	1719	24%	1713	23%
Number of bonded IOBs	40	8%	90	25%
Number of BlockRAM/FIFO	2	3%	1	1%
Number of BUFG/BUFGCTRLs	7	21%	10	31%
Number of DSP48Es	NA	NA	32	66%
Total equivalent gate count	275,214	NA	195438	NA

Chapter 3

System Test

3.1   DAC Interpolating Filter Measurement

The equivalent baseband filter in the transmitter-receiver chain has to be taken into account in order to have optimum waveform at the receiver detector. This filter is generally not flat over the frequency band of interest, especially for wide bandwidth case. Estimating and controlling the equivalent baseband filter is not easy. As shown in Fig. 3.1, the overall filter effect is contributed from three sources: the DAC's interpolating filter $p(t)$ and RF front-ends including antennas at both sides. By omitting some scalar factor, the equivalent filter in baseband format is

$$F(t) = F_0(t) \otimes F_1(t) \otimes F_2(t), \tag{3.1}$$

and $F_0(t)$ can be expressed using the interpolating filter $p(t)$

$$F_0(t) = p(t) + j \cdot p(t). \tag{3.2}$$

According to our measurement, the shape of the equivalent filter is dominated by the interpolating filter $p(t)$. Based on the ADC used in the testbed, $p(t)$ has been accurately measured and $F_0(t) = p(t) + j \cdot p(t)$ has been used as an estimate of $F(t)$.

To measure the filter, a full scale (14-bit) 1-ns wide digital pulse directly generated in the FPGA chip is used as a trigger source, resulting in a analog pulse at the DAC's output. This pulse, as shown in Fig. 3.2, is actually the interpolating pulse shape (filter) corresponding to sampling rate of 1 Gs/s. The pulse width is over 1 ns and there is a tail behind the pulse, implying imperfect circuit coupling. The spectrum of the interpolating filter is depicted in Fig. 3.3.
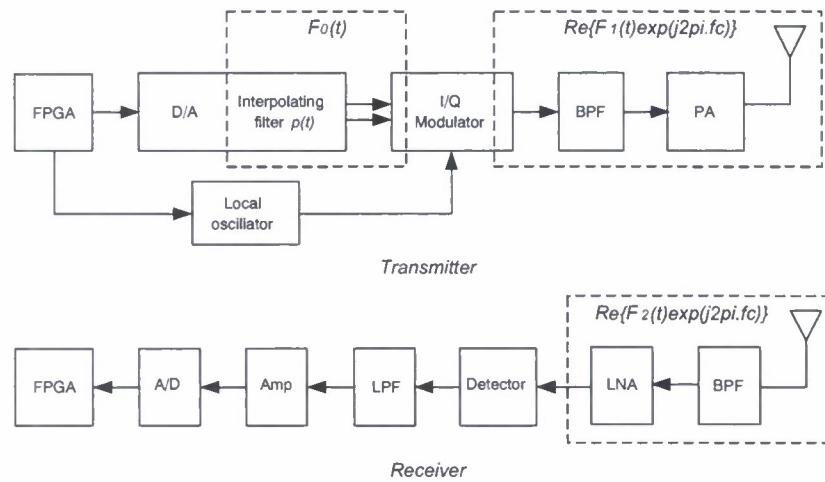
Figure 3.1: Equivalent filter in transmitter-receiver chain (not including the propagation channel), contributed from three sources.
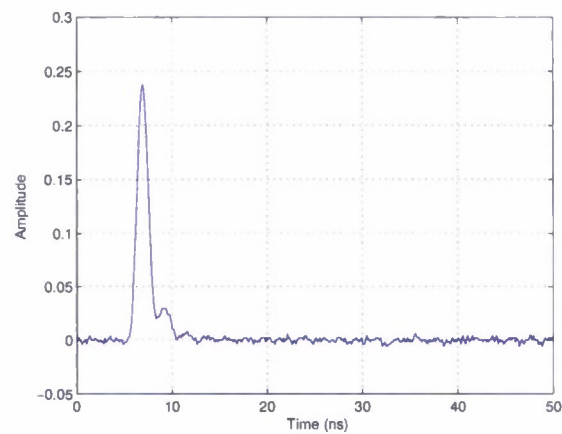

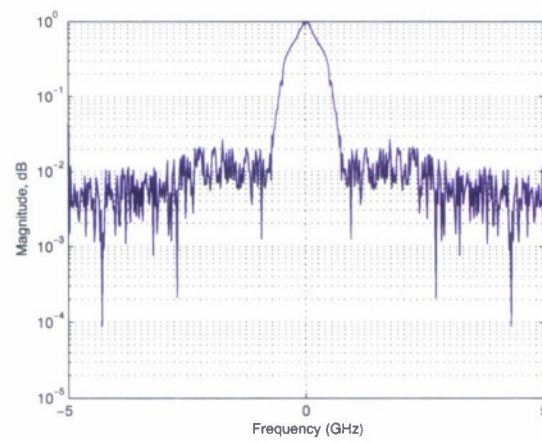Figure 3.2: Measured interpolating pulse shape.

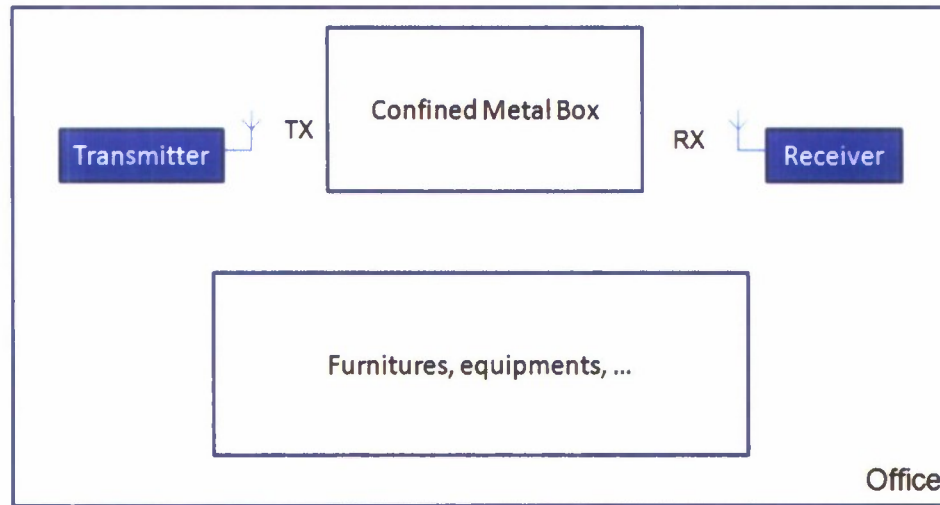Figure 3.3: The spectrum of the interpolating filter.

Figure 3.4: Layout for measurement in metal box.

3.2 Performance Measurement

The system was tested in a typical officc/lab, non-line-of-sight (NLOS) environment. The layout for office/lab environment is illustrated in Fig. 3.4. The transmitter and the receiver are set in onc room, blocked by a confined metallic box. The height of both antennas is about 1.5 m. Separation distance between the two antennas is not a good metric since the path loss and the multipath profile do not solely depend upon the distance. The path loss in this scenario is over 70 dB. Two 30 dB low-noise-amplifiers (LNA) are used to compensate the path loss at the transmitter and recciver, respectively.

We first use vector nctwork analyzer (VNA) to measure the channel and get the Time Reversal I/Q waveforms via the method mentioned in the January report. Fig. 3.5 shows channel transfer function (CTF) and Fig. 3.6 shows the I/Q modulation waveforms. Before loading the trimmed Time Reversal waveforms into FPGA, we load the full-length waveforms to the DAC's waveform memory to verify the validity of Time Reversal. If a focused signal can be observed at the receiver, then we say the waveforms are correct. It can be easily observed that only the Time Reversal one is focused in time.

Trimmed waveforms are loaded in FPGA to conduct the system trial. Receiver sensitivity is measured in this trial. We reduce the transmit power until the receiver can not detect any signal. Based on this criterion, it is found that with insignificant ISI, the recciver sensitivity (measured in average receive power) for the time reversal is around -81 dBm. The transmit spectra of Time Reversal system and impulse system are depicted in Fig. 3.7 and their powers are 6.1 dBm and 8.9 dBm respectively. The receivc spectra of Time Reversal system and impulse system are depicted in Fig. 3.8 and both of the powers are -81 dBm. As a result, Time Reversal system has a 2.8 dB gain from the channel over impulse system.
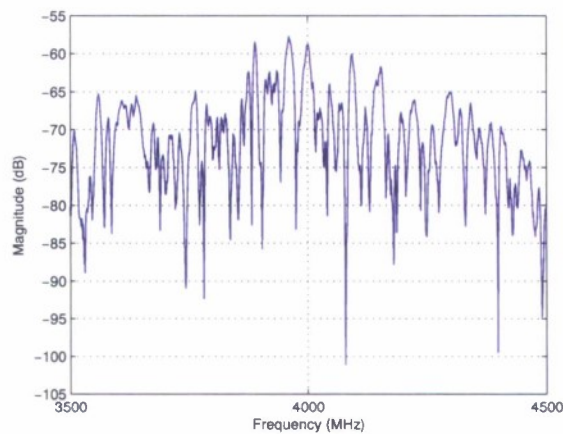
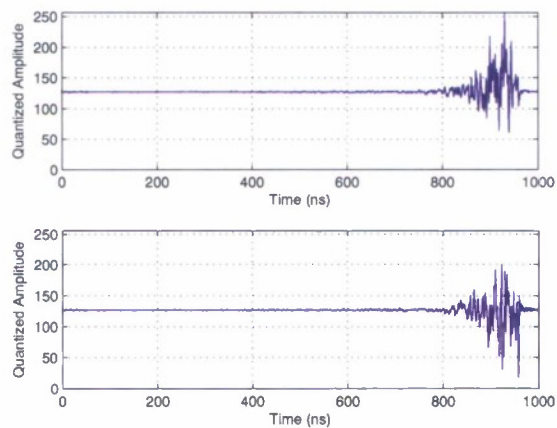Figure 3.5: Channel transfer function, measured data from VNA.

Figure 3.6: Quantized I/Q modulation waveforms for DAC. Top is the I channel waveform and bottom is the Q channel waveform.
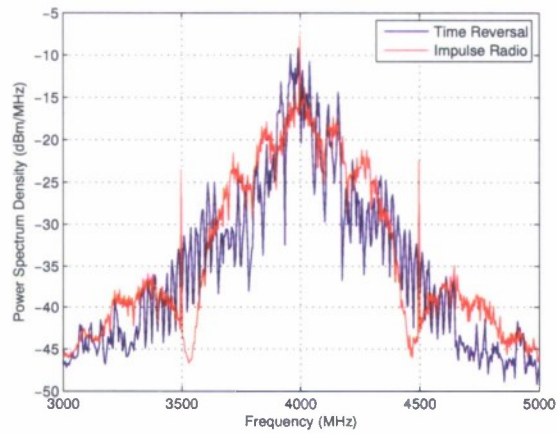
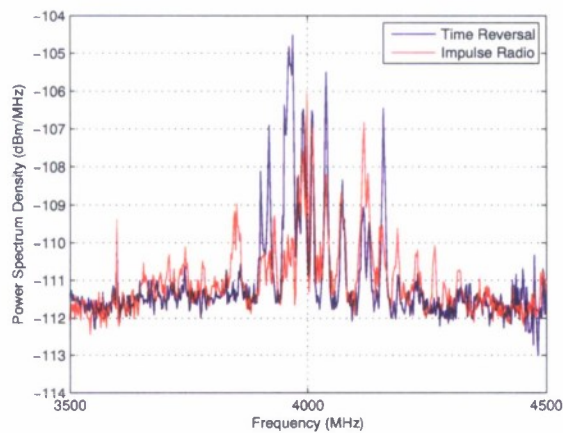Figure 3.7: Transmit speetra for Time Reversal system and impulse radio system.

Figure 3.8: Reeeive speetra for Time Reversal system and impulse radio system.

Chapter 4

Current and Near-Future Work

Although a gain contributed by time reversal precoding has been achieved, we believe there are still some room to improve the hardware implementation and the performance. Moreover, we have started to design a new test-bed with compressive sensing capability.

4.1 Synchronization Optimization

The proposed 3-stage synchronization scheme follows proper design philosophy for burst mode communication. We have found that the synchronization performance varies depending on the system configuration. There are a number of parameters that may need to be optimized. However, globally optimizing the overall synchronization performance is too challenging. A practical optimization strategy is to combine pure analysis, measurement and simulation. A detailed methodology needs to be investigated before starting the optimization process.

4.2 Newer DAC and ADC

The DAC (MAX108) used in the receiver is not ideal in terms of sampling rate and connection. We are planning to replace it with some newer product to reach a sampling rate of 2 Gs/s or above. Current the sampling rate is only 800 Ms/s, which might cause performance degradation since the time reversal pulse width at the detector's output is only 6 ns at the half height. If the sampling rate increases to 2 Gs/s, 12 samples can be effectively captured for each received pulse. The current connection between the ADC and the FPGA board is loose and the individual path lengths for different bits of a sample are not accurately aligned mainly due to physical PCB routing limitation in the cable-connector adapting PCB.

A high speed ribbon cable/bus has been successfully used to connect the DAC and the FPGA board in the transmitter. However, It is doubtable for this type of cables to meet our higher sampling rate requirement. One solution to the bottleneck caused by connection is to use a signal processing package with an ADC (or a DAC) and an FPGA chip integrated on a single board. We are searching such type of boards and evaluating their performance to price ratios.

4.3   Non-coherent Threshold-less Detection

OOK modulation has been adopted in the system mainly for its simplicity for non-coherent detection. The number one bothering problem in the system with OOK modulation and non-coherent detection is the sensitivity to the decision threshold. An optimum threshold depends on the SNR at the receiver, and it requires sophisticated signal processing to achieve the optimum, which prevents the performance from being the optimum practically.

Per above discussion, non-coherent threshold-less detection is extremely desired. One solution is a combination of PPM modulation and non-coherent detection. Shown in Fig.4.1 is a conceptual receiver block diagram for PPM modulation with non-coherent detection.
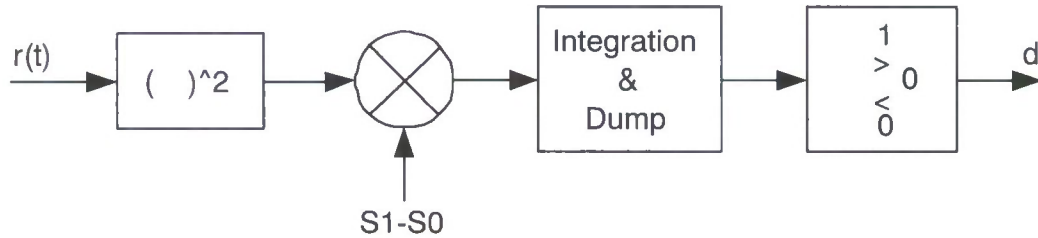
Figure 4.1: Conceptual receiver block diagram for PPM modulation with non-coherent detection

4.4   2-by-1 MISO

A 3-dB array gain can be anticipated if the number of transmitter branches increases from one to two. For the passband signaling approach, the carriers in the two branches must be strictly aligned, which requires identical DACs, modulators and power amplifiers in the both branches. The two branches can share a common local oscillator (LO). We are currently searching devices for this matter.

4.5   Direct-Conversion Receiver

To explore more communication techniques, especially those implemented at receiver side, a coherent receiver will provide more potential than a non-coherent receiver. Among all coherent receiver architectures is a direct-conversion receiver which is popular nowadays. This type of receiver is also called homodyne, synchrodyne or zero-IF receiver. An attractive feature of a direct-conversion receiver is that it requires less analog processing but more digital processing. This feature favors our design philosophy in terms of flexibility, thus it has been considered as our new receiver. In UWB band, a modulation-demodulation scheme to test on this receiver might be transmitted reference or its variants.

4.6 Real-Time Error Rate Measurement

So far we have tested frame loss rate (due to synchronization failure) and bit error rate in a non-real-time way. A real-time error meter will be extremely desired since it can serve as an indicator in a system trial and make the measurement more efficient and effective. A stand-alone real-time error meter mainly consists of a data acquisition section as well as a data processing section, and it can be virtually used in different situations. A difficult part of a stand-alone error meter is to synchronize the meter with the incoming data stream.

4.7   Implementation of a Compressed Sensing Based Communication System

We propose an implementable Compressed Sensing (CS) based communication system, as illustrated in Fig. 4.2. A 1 Ghz UWB signal is transmitted in the 10 GHz carrier and captured by a 25 Msps A/D. This system utilizes the concept in the October 2008's report but with smaller bandwidth. This is due to the limitation of available RF hardware. The baseband signal must be modulated to carrier frequency because no antennas can transmit signal with frequency starting from DC. Sparse pulse position modulation (PPM) data is digitally filtered by a high rate PN filter in FPGA. For a Xilinx Virtex 5 FPGA, the rate of output signal can be up to 3.2 Gsps thanks to the advanced RocketIO technology. The circuity in FPGA acts as a virtual interpolating filter, transforming digital signal into analog waveform. Alternatively, we can build a PN sequence generator with rate up to even 80 Gsps by standard high rate shift register. However, this is not implementable due to the limitation of the state-of-art RF technology. To the best knowledge of the author, the largest bandwidth supported by a modulator is 1 GHz, provided by MITEQs SDM1015LI3CDQ with 10 GHz - 15 GHz RF output. As a result, the output signal bandwidth from FPGA should not exceed 1 GHz. Power amplifier (PA) is used before transmitting the UWB signal over the air. The structure of the receiver is very simple. There is no down-conversion. A 25 Msps A/D samples the data directly after a low noise amplifier (LNA) and passband filter. FPGA is used to acquire the A/D data and process with recovery algorithms such as OMP, StOMP, etc..

The following is a list of key hardware found in the market in Fig. 4.2:

- FPGA: Xilinx Virtex 5 LX330T with 3.25 Gsps RocketIO

- Modulator: MITEQ SDM1015LI3CDQ with 1 GHz modulation bandwidth, 10 GHz - 15 Ghz RF output frequency

- Local Oscillator: MITEQ LPLM15000 with 8 GHz - 15 GHz output frequency

- PA: MITEQ AMF-6B-08001800-60-34P with 8 GHz - 18 GHz frequency range, 37 dB gain

- LNA: MITEQ AMFW-5S-10001500-250 with 10 GHz - 15 GHz frequency range, 30 dB gain
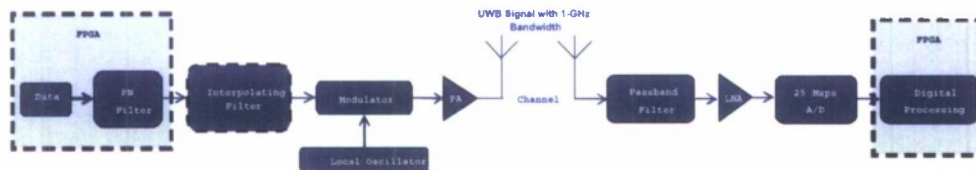

Figure 4.2: Architecture of a proposed compressed sensing based communication system.

Part II

Theoretical Work

Chapter 5

Wideband Waveform Optimization with Energy Detector Receiver in Cognitive Radio

5.1 Introduction

Waveform design or optimization is a key research issue in the current wireless communication system. Waveform should be designed according to the different requirements and objectives of system performance. For example, the waveform should be designed to carry more information to the receiver in terms of capacity. For navigation and geolocation, the ultra short waveform should be used to increase the resolution. If the energy detector is employed at the receiver, the waveform should be optimized such that the energy of the signal within integration window at the receiver should be maximized. In the context of cognitive radio, waveform design or optimization gives us more flexibility to design a radio which can coexist with other cognitive radios and primary radios. From cognitive radio's point of view, spectral mask constraint at the transmitter and the influence of Arbitrary Notch Filter at the receiver should be seriously considered for waveform design or optimization, except the consideration of the traditional communication objectives. Spectral mask constraint is imposed on the transmitted waveform such that cognitive radio has no interference to primary radio. While Arbitrary Notch Filter at the receiver is used to cancel the interference from primary radio to cognitive radio. Though Arbitrary Notch Filter is at the receiver, the influence of Arbitrary Notch Filter should be incorporated into waveform design at the transmitter. How to implement Arbitrary Notch Filter is out of scope of this chapter.

The optimization problem is formulated as Quadratically Constrained Quadratic Program (QCQP), which is known as an NP-hard problem. However, after relaxation, QCQP can be solved by using Semidefinite Program (SDP) plus a randomized algorithm. In addition to SDP, a computationally-efficient iterative method is proposed to give the optimal solution for a special situation where the integrator only captures one sample after ADC as the decision statistic.

5.2 System Description and Optimal Waveform

The system architecture is shown in Figure 5.1. We limit our discussion to a single-user scenario, and consider the transmitted signal with OOK modulation given by

$$s(t) = \sum_{j=-\infty}^{\infty} d_j p(t - jT_b) \tag{5.1}$$

where T_b is the symbol duration, $p(t)$ is the transmitted symbol waveform defined over $[0, T_p]$ and $d_j \in \{0, 1\}$ is the j-th transmitted bit. Without loss of generality, assume the minimal propagation delay is equal to zero. The energy of $p(t)$ is E_p,

$$\int_0^{T_p} p^2(t)\, dt = E_p \tag{5.2}$$

and the frequency domain representation of $p(t)$ is $p_f(f)$. Thus,

$$\int_{-\infty}^{\infty} |p_f(f)|^2\, df = E_p \tag{5.3}$$

The received noise-polluted signal at the output of low noise amplifier (LNA) is

$$r(t) = h(t) \otimes s(t) + n(t) \tag{5.4}$$

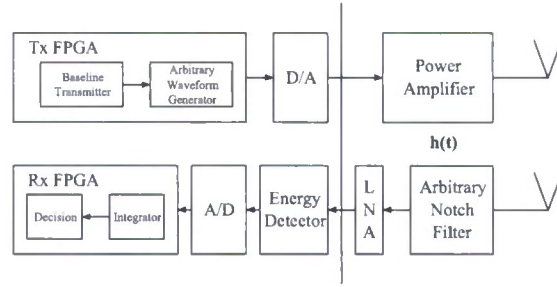$$= \sum_{j=-\infty}^{\infty} d_j x(t - jT_b) + n(t) \tag{5.5}$$

Figure 5.1: System architecture.

where $h(t), t \in [0, T_h]$ is the multipath impulse response that takes into account the effect of channel impulse response, the RF front-ends in the transceivers such as Power Amplifier, LNA and Arbitrary Notch Filter as well as antennas. $h(t)$ is available at the transmitter [1] [2] and the energy of $h(t)$ is E_h,

$$\int_0^{T_h} h^2(t) \, dt = E_h \tag{5.6}$$

and the frequency domain representation of $h(t)$ is $h_f(f)$. Thus,

$$\int_{-\infty}^{\infty} |h_f(f)|^2 \, df = E_h \tag{5.7}$$

"$\otimes$" denotes convolution operation. $n(t)$ is a low-pass additive zero-mean Gaussian noise with one-sided bandwidth W and one-sided power spectral density N_0. $x(t)$ is the received noiseless symbol-"1" waveform defined as

$$x(t) = h(t) \otimes p(t) \tag{5.8}$$

We further assume that $T_b \geq T_h + T_p \stackrel{\text{def}}{=} T_x$, i.e. no existence of ISI.

An energy detector performs square operation to $r(t)$. Then the integrator does the integration over a given integration window T_I. Corresponding to the time index k, the k-th decision statistic at the output of the integrator is given by

$$z_k = \int_{kT_b+T_{I0}}^{kT_b+T_{I0}+T_I} r^2(t) dt \tag{5.9}$$

$$= \int_{kT_b+T_{I0}}^{kT_b+T_{I0}+T_I} (d_k x(t - kT_b) + n(t))^2 dt \tag{5.10}$$

where T_{I0} is the starting time of integration for each symbol and $0 \leq T_{I0} < T_{I0} + T_I \leq T_x \leq T_b$.

An approximately equivalent SNR for the energy detector receiver, which provides the same detection performance when applied to a coherent receiver, is given as [3]

$$\text{SNR}_{\text{eq}} = \frac{2 \left(\int_{T_{I0}}^{T_{I0}+T_I} x^2(t) \, dt \right)^2}{2.3 T_I W N_0^2 + N_0 \int_{T_{I0}}^{T_{I0}+T_I} x^2(t) \, dt} \tag{5.11}$$

For best performanee, the equivalent SNR SNR_{eq} should be maximized. Define,

$$E_I = \int_{T_{I0}}^{T_{I0}+T_I} x^2\left(t\right) dt \tag{5.12}$$

For given T_I, N_0 and W, SNR_{eq} is the increasing funetion of E_I. So the maximization of SNR_{eq} in Equation 5.11 is equivalent to the maximization of E_I in Equation 5.12.

So the optimization problem to get the optimal $p(t)$ is shown below,

$$\begin{aligned} \max \int_{T_{I0}}^{T_{I0}+T_I} x^2\left(t\right) dt \\ s.t. \int_0^{T_p} p^2\left(t\right) dt = E_p \end{aligned} \tag{5.13}$$

In order to solve the optimization problcm 5.13, a numerical approach is employed in this document. In other words, $p(t)$, $h(t)$ and $x(t)$ are uniformly sampled (assumed at Nyquist rate), and the optimization problem 5.13 will be eonverted to its eorresponding diserete-time form. Assume the sampling period is T_s. $T_p/T_s = N_p$ and N_p is assumed to be even, $T_h/T_s = N_h$ and $T_x/T_s = N_x$. So $N_x = N_p + N_h$.

$p(t)$, $h(t)$ and $x(t)$ are represented by $p_i, i = 0, 1, \ldots, N_p$, $h_i, i = 0, 1, \ldots, N_h$ and $x_i, i = 0, 1, \ldots, N_x$ respee-tivcly [3].

Define,

$$\mathbf{p} = [p_0 \ p_1 \ \cdots \ p_{N_p}]^T \tag{5.14}$$

and

$$\mathbf{x} = [x_0 \ x_1 \ \cdots \ x_{N_x}]^T \tag{5.15}$$

Construet channel matrix $\mathbf{H}_{(N_x+1)\times(N_p+1)}$,

$$(\mathbf{H})_{i,j} = \begin{cases} h_{i-j}, 0 \le i - j \le N_h \\ 0, \quad else \end{cases} \tag{5.16}$$

where $(\bullet)_{i,j}$ denotes the cntry in the i-th row and j-th eolumn of the matrix or veetor. Meanwhile, for veetor, taking $\mathbf{p}$ as an example, $(\mathbf{p})_{i,1}$ is equivalent to p_{i-1}.

The matrix expression of Equation 5.8 is,

$$\mathbf{x} = \mathbf{Hp} \tag{5.17}$$

and the constraint in the optimization problem 5.13 can be expressed as,

$$\|\mathbf{p}\|_2^2 T_s = E_p \tag{5.18}$$

where "$\|\bullet\|_2$" denotes the norm-2 of the vector. In order to make the whole doeument eonsistent, we further assume,

$$\|\mathbf{p}\|_2^2 = 1 \tag{5.19}$$

Let $T_I/T_s = N_I$ and $T_{I0}/T_s = N_{I0}$. The entries in $\mathbf{x}$ within integration window constitute $\mathbf{x}_I$ as,

$$\mathbf{x}_I = [x_{N_{I0}} \ x_{N_{I0}+1} \ \cdots \ x_{N_{I0}+N_I}]^T \tag{5.20}$$

and E_I in Equation 5.12 can be equivalently shown as,

$$E_I = \|\mathbf{x}_I\|_2^2 \, T_s \tag{5.21}$$

Simply dropping T_s in E_I will not affect the optimization objective, so E_I is redefined as,

$$E_I = \|\mathbf{x}_I\|_2^2 \tag{5.22}$$

Similar to Equation 5.17, $\mathbf{x}_I$ can be obtained by,

$$\mathbf{x}_I = \mathbf{H}_I \mathbf{p} \tag{5.23}$$

where $(\mathbf{H}_I)_{i,j} = (\mathbf{H})_{N_{I0}+i,j}$ and $i = 1, 2, \ldots, N_I + 1$ as well as $j = 1, 2, \ldots, N_p + 1$.

The optimization problem 5.13 can be represented by its discrete-time form as,

$$\begin{aligned} \max \; & E_I \\ s.t. \; & \|\mathbf{p}\|_2^2 = 1 \end{aligned} \tag{5.24}$$

The optimal solution $\mathbf{p}^*$ for the optimization problem 5.24 is the dominant eigen-vector in the following eigen-function [3],

$$\mathbf{H}_I^T \mathbf{H}_I \mathbf{p} = \lambda \mathbf{p} \tag{5.25}$$

Furthermore, E_I^* will be obtained by Equation 5.22 and Equation 5.23.

5.3 Wideband Waveform Design in Cognitive Radio

For cognitive radio, there is a spectral mask constraint for the transmitted waveform. Based on the previous discussion, $\mathbf{p}$ is assumed to be the transmitted waveform and $\mathbf{F}$ is the Fourier transform matrix, thus the frequency domain representation of $\mathbf{p}$ is,

$$\mathbf{p}_f = \mathbf{F}\mathbf{p} \tag{5.26}$$

where $\mathbf{p}_f$ is a complex value vector. If the i-th row of $\mathbf{F}$ is $\mathbf{f}_i$, then each complex value in $\mathbf{p}_f$ can be represented by,

$$(\mathbf{p}_f)_{i,1} = \mathbf{f}_i \mathbf{p}, i = 1, 2, \ldots, \frac{N_p}{2} + 1 \tag{5.27}$$

Thus the modulus of the complex value is $|\bullet|$.

Define,

$$\mathbf{F}_i = \mathbf{f}_i^H \mathbf{f}_i, i = 1, 2, \ldots, \frac{N_p}{2} + 1 \tag{5.28}$$

Given the spectral mask constraint in terms of power spectral density $\mathbf{c} = \left[c_1 \, c_2 \cdots c_{\frac{N_p}{2}+1} \right]^T$, so

$$\begin{aligned} \left| (\mathbf{p}_f)_{i,1} \right|^2 &= |\mathbf{f}_i \mathbf{p}|^2 \tag{5.29} \\ &= \mathbf{p}^T \mathbf{f}_i^H \mathbf{f}_i \mathbf{p} \tag{5.30} \\ &= \mathbf{p}^T \mathbf{F}_i \mathbf{p} \tag{5.31} \\ &\leq c_i, i = 1, 2, \ldots, \frac{N_p}{2} + 1 \tag{5.32} \end{aligned}$$

So the optimization problem with spectral mask constraint can be expressed as,

$$
\max E_I
$$
$$
s.t. \quad
\begin{aligned}
\|\mathbf{p}\|_2^2 &\leq 1 \\
\mathbf{p}^T \mathbf{F}_1 \mathbf{p} &\leq c_1 \\
&\vdots \\
\mathbf{p}^T \mathbf{F}_{\frac{N_p}{2}+1} \mathbf{p} &\leq c_{\frac{N_p}{2}+1}
\end{aligned}
\tag{5.33}
$$

Define,

$$
\mathbf{H}_o = \mathbf{H}_I^T \mathbf{H}_I
\tag{5.34}
$$

Equation 5.22, Equation 5.23 and Equation 5.34 are put into the optimization problem 5.33, and then this optimization problem will be formulated as,

$$
\max \mathbf{p}^T \mathbf{H}_o \mathbf{p}
$$
$$
s.t. \quad
\begin{aligned}
\mathbf{p}^T \mathbf{p} &\leq 1 \\
\mathbf{p}^T \mathbf{F}_1 \mathbf{p} &\leq c_1 \\
&\vdots \\
\mathbf{p}^T \mathbf{F}_{\frac{N_p}{2}+1} \mathbf{p} &\leq c_{\frac{N_p}{2}+1}
\end{aligned}
\tag{5.35}
$$

In the optimization problem 5.35, both the objective function and the constraints are quadratic functions, so this kind of optimization problem is a QCQP. The general QCQP is a NP-hard problem. A semidefinite relaxation method is used in this document to give the suboptimal solution to the optimization problem 5.35.

Define,

$$
\mathbf{P} = \mathbf{p}\mathbf{p}^T
\tag{5.36}
$$

So $\mathbf{P}$ should be the symmetric positive semidefinite matrix, i.e. $\mathbf{P} \succeq = 0$ and rank of $\mathbf{P}$ should be equal to 1.

Then,

$$
\begin{aligned}
E_I &= \mathbf{p}^T \mathbf{H}_o \mathbf{p} & (5.37) \\
&= \text{trace}\left(\mathbf{H}_o \mathbf{p}\mathbf{p}^T\right) & (5.38) \\
&= \text{trace}\left(\mathbf{H}_o \mathbf{P}\right) & (5.39)
\end{aligned}
$$

and $\|\mathbf{p}\|_2^2 = \text{trace}(\mathbf{P})$, $\mathbf{p}^T \mathbf{F}_i \mathbf{p} = \text{trace}(\mathbf{F}_i \mathbf{P})$, $i = 1, 2, \ldots, \frac{N_P}{2} + 1$.

Rank constraint is nonconvex constraint, so after dropping it, QCQP is relaxed to SDP,

$$
\max \text{trace}\left(\mathbf{H}_o \mathbf{P}\right)
$$
$$
s.t. \quad
\begin{aligned}
\text{trace}\left(\mathbf{P}\right) &\leq 1 \\
\text{trace}\left(\mathbf{F}_1 \mathbf{P}\right) &\leq c_1 \\
&\vdots \\
\text{trace}\left(\mathbf{F}_{\frac{N_P}{2}+1} \mathbf{P}\right) &\leq c_{\frac{N_p}{2}+1}
\end{aligned}
\tag{5.40}
$$

The optimal solution $\mathbf{P}^*$ of the optimization problem 5.40 can be obtained by using CVX tool [4] and the value of the objective function gives the upper bound of the optimal value in the optimization problem 5.35. If the rank of

$\mathbf{P}^*$ is equal to 1, then the dominant eigen-vector of $\mathbf{P}^*$ will be the optimal solution $\mathbf{p}^*$ for the optimization problem 5.35. But if the rank of $\mathbf{P}^*$ is not equal to 1, the dominant eigen-vector of $\mathbf{P}^*$ can not be treated as the optimal solution for the optimization problem 5.35, because of the violation of bound constraint.

An efficient randomized algorithm is given by [5] [6] to obtain the feasible solution $\mathbf{p}^*$ from $\mathbf{P}^*$.

This algorithm will be repeated a sufficient number of times to get the relatively good feasible $\mathbf{p}^*$ as the suboptimal solution to the optimization problem 5.35.

When T_I approaches zero, which means the integrator only captures one sample after ADC as the decision statistic, the maximization of E_I will be equivalent to the maximization of $x\,(T_{I0})$. An iterative algorithm is proposed here to give the solution to the maximization of $x\,(T_{I0})$, which will be more computationally efficient than the previous semidefinite relaxation method. For the simplicity of the following presentation, T_{I0} is assumed to be zero.

From the inverse Fourier transform,

$$x\,(t) = \int_{-\infty}^{\infty} x_f\,(f)\,e^{j2\pi ft}df \tag{5.41}$$

and from Equation 5.8,

$$x_f\,(f) = h_f\,(f)\,p_f\,(f) \tag{5.42}$$

where $x_f\,(f)$ is the the frequency domain representation of $x(t)$ respectively.

So,

$$x\,(0) \;=\; \int_{-\infty}^{\infty} x_f\,(f)\,df \tag{5.43}$$

$$\;=\; \int_{-\infty}^{\infty} h_f\,(f)\,p_f\,(f)\,df \tag{5.44}$$

If there is no spectral mask constraint, then according to the Cauchy$-$Schwarz inequality,

$$x\,(0) \;=\; \int_{-\infty}^{\infty} h_f\,(f)\,p_f\,(f)\,df \tag{5.45}$$

$$\;\leq\; \sqrt{\int_{-\infty}^{\infty} |h_f\,(f)|^2\,df \int_{-\infty}^{\infty} |p_f\,(f)|^2\,df} \tag{5.46}$$

$$\;=\; \sqrt{E_h E_p} \tag{5.47}$$

when $p_f\,(f) = \alpha h_f^*\,(f)$ for all f, the equality is obtained. In this case, $p(t) = \alpha h(-t)$, which means the optimal waveform is the time reversed multipath impulse response. And,

$$\alpha = \sqrt{\frac{E_p}{E_h}} \tag{5.48}$$

If there is a spectral mask constraint, then the following optimization problem will become more complicated.

$$\begin{aligned} &\max x\,(0)\\ &s.t. \int_{-\infty}^{\infty} |p_f\,(f)|^2\,df \leq 1\\ &\quad\;\; |p_f\,(f)|^2 \leq c_f\,(f) \end{aligned} \tag{5.49}$$

where $c_f(f)$ represents the arbitrary spectral mask constraint.

Because $p_f(f)$ is the complex value, the phase and the modulus of $p_f(f)$ should be determined.

$$x(0) = \int_{-\infty}^{\infty} h_f(f) p_f(f) df \tag{5.50}$$

$$= \int_{-\infty}^{\infty} |h_f(f)| e^{j2\pi \arg(h_f(f))} |p_f(f)| e^{j2\pi \arg(p_f(f))} df \tag{5.51}$$

$$= \int_{-\infty}^{\infty} |h_f(f)| |p_f(f)| e^{j2\pi(\arg(h_f(f))+\arg(p_f(f)))} df \tag{5.52}$$

where the angular component of the complex value is $\arg(\bullet)$.

For the real value signal $x(t)$,

$$x_f(f) = x_f^*(-f) \tag{5.53}$$

where "$*$" denotes conjugate operation.

$$x_f(f) = |h_f(f)| |p_f(f)| e^{j2\pi(\arg(h_f(f))+\arg(p_f(f)))} \tag{5.54}$$

$$x_f(-f) = |h_f(f)| |p_f(f)| e^{-j2\pi(\arg(h_f(f))+\arg(p_f(f)))} \tag{5.55}$$

and $x_f(f) + x_f(-f)$ is equal to

$$|h_f(f)| |p_f(f)| \cos(2\pi(\arg(h_f(f)) + \arg(p_f(f)))) \tag{5.56}$$

If $h(f)$ and $|p_f(f)|$ is given, maximization of $x(0)$ is equivalent to setting,

$$\arg(h(f)) + \arg(p(f)) = 0 \tag{5.57}$$

which means the angular component of $p_f(f)$ is the negative angular component of $h_f(f)$.

The optimization problem 5.49 can be simplified as,

$$\begin{aligned} &\max \int_{-\infty}^{\infty} |h_f(f)| |p_f(f)| df \\ &s.t. \int_{-\infty}^{\infty} |p_f(f)|^2 df \leq 1 \\ &|p_f(f)|^2 \leq c_f(f), f \geq 0 \end{aligned} \tag{5.58}$$

Because,

$$|h_f(f)| = |h_f(-f)| \tag{5.59}$$

$$|p_f(f)| = |p_f(-f)| \tag{5.60}$$

$$|c_f(f)| = |c_f(-f)| \tag{5.61}$$

for all f. Thus uniformly discrete frequency points $f_0, \ldots, f_M$ are considered in the optimization problem 5.58. Meanwhile, f_0 corresponds to the DC component and $f_1, \ldots, f_M$ correspond to the positive frequency component.

Define vector $\mathbf{h}_f$,

$$(\mathbf{h}_f)_{i,1} = \begin{cases} |h_f(f_{i-1})|, i = 1 \\ \sqrt{2} |h_f(f_{i-1})|, i = 2, \ldots, \frac{N_p}{2} + 1 \end{cases} \tag{5.62}$$

Define vector $\mathbf{p}_f$,

$$(\mathbf{p}_f)_{i,1} = \begin{cases} |p_f(f_{i-1})|, i = 1 \\ \sqrt{2}|p_f(f_{i-1})|, i = 2, \ldots, \frac{N_p}{2} + 1 \end{cases} \qquad (5.63)$$

Define vector $\mathbf{c}_f$

$$(\mathbf{c}_f)_{i,1} = \begin{cases} \sqrt{c_f(f_{i-1})}, i = 1 \\ \sqrt{2c_f(f_{i-1})}, i = 2, \ldots, \frac{N_p}{2} + 1 \end{cases} \qquad (5.64)$$

Thus, the discrete version of the optimization problem 5.58 is shown below,

$$\begin{aligned} \max \mathbf{h}_f^T \mathbf{p}_f \\ s.t. \|\mathbf{p}_f\|_2^2 \leq 1 \\ \mathbf{p}_f \leq \mathbf{c}_f \end{aligned} \qquad (5.65)$$

So an iterative algorithm is proposed to get the optimal solution $\mathbf{p}_f^*$ to the optimization problem 5.65 as follows.

1. Initialization: $P = 1$ and $\mathbf{p}_f^*$ is set to be an all-0 column vector.

2. Solve the following optimization problem to get the optimal $\mathbf{q}_f^*$ using Cauchy$-$Schwarz inequality.

$$\begin{aligned} \max \mathbf{h}_f^T \mathbf{q}_f \\ s.t. \|\mathbf{q}_f\|_2^2 \leq P \end{aligned} \qquad (5.66)$$

3. Find i, such that $\left(\mathbf{q}_f^*\right)_{i,1}$ is the maximal value in the set $\left\{ \left(\mathbf{q}_f^*\right)_{j,1} \Big| \left(\mathbf{q}_f^*\right)_{j,1} > (\mathbf{c}_f)_{j,1} \right\}$. If $\{i\} = \emptyset$, then the algorithm is terminated and $\mathbf{p}_f^* := \mathbf{p}_f^* + \mathbf{q}_f^*$. Otherwise go to step 4.

4. Set $\left(\mathbf{p}_f^*\right)_{i,1} = (\mathbf{c}_f)_{i,1}$.

5. $P := P - (\mathbf{c}_f)_{i,1}^2$ and set $(\mathbf{h}_f)_{i,1}$ to zero. Go to step 2.

When $\mathbf{p}_f^*$ is obtained for the optimization problem 5.65, from Equation 5.57 and Equation 5.63, the optimal $p_f(f)$ and the corresponding $p(t)$ can be smoothly achieved.

The proposed iterative algorithm gives the optimal solution to the optimization problem 5.65, which can be proofed as follows.

Given column vector $\mathbf{a}$, all the entries $a_1, \ldots, a_N$ in $\mathbf{a}$ are positive. Meanwhile, we assume $a_1 > \max\{a_2, \ldots, a_N\}$. We would like to solve the following optimization problem to get the optimal column vector $\mathbf{b}$,

$$\begin{aligned} \max \mathbf{a}^T \mathbf{b} \\ s.t. \mathbf{b}^T \mathbf{b} \leq P \\ b_1 < c \\ c < \frac{a_1 \sqrt{P}}{\sum_{i=1}^{N} a_i^2} \end{aligned} \qquad (5.67)$$

For optimal solution $\mathbf{b}^*$, if $b_1^* = c$, then the optimum of the iterative algorithm is achieved. Set $b_1 = \alpha c$, where $0 \le \alpha \le 1$, then,

$$\mathbf{a}^T \mathbf{b} = \sum_{i=1}^{N} a_i b_i \tag{5.68}$$

$$= a_1 b_1 + \sum_{i=2}^{N} a_i b_i \tag{5.69}$$

$$\le \alpha a_1 c + \sqrt{\sum_{i=2}^{N} a_i^2} \sqrt{P - \alpha^2 c^2} \tag{5.70}$$

Let $f(\alpha) = \alpha a_1 c + \sqrt{\sum_{i=2}^{N} a_i^2} \sqrt{P - \alpha^2 c^2}$, the optimization problem is reduced to,

$$\begin{aligned} \max f(\alpha) \\ s.t. 0 \le \alpha \le 1 \end{aligned} \tag{5.71}$$

From $f(\alpha)$, we can get $\frac{df}{d\alpha}(\alpha)$,

$$\frac{df}{d\alpha}(\alpha) = a_1 c - \frac{\alpha c^2 \sqrt{\sum_{i=2}^{N} a_i^2}}{\sqrt{P - \alpha^2 c^2}} \tag{5.72}$$

Let $\frac{df}{d\alpha}(\alpha)$ is equal to zero, then α is equal to $\pm \frac{a_1 \sqrt{P}}{c \sum_{i=1}^{N} a_i^2}$. Because of the constraint on c, $|\alpha|$ is greater than 1.

Meanwhile, $\frac{df}{d\alpha}(0) = a_1 c$, which means $\frac{df}{d\alpha}(\alpha)$ keeps positive value in $[0, 1]$. Thus $f(\alpha)$ is a monotone increasing function in $[0, 1]$. $\arg \max_{\alpha \in [0,1]} f(\alpha) = 1$. So, $b_1 = c$. The optimum of the iterative algorithm is verified.

5.4   Numerical Results

Figure 5.2 shows the multipath impulse response $h(t)$ under investigation in this document and the energy of $h(t)$ is normalized. Figure 5.3 shows the frequency domain representation $h_f(f)$ of $h(t)$. Green notch line in Figure 5.3 shows the influence of Arbitrary Notch Filter at the receiver. $T_s = 0.5ns$, $T_h = 100ns$, $T_p = 100ns$ and $T_{I0} + \frac{T_I}{2} = 100ns$. In the following presentation, the designed waveform, which is obtained by SDP and the rank of $\mathbf{P}^*$ to the optimization problem 5.40 is not equal to 1, is called Waveform SDP Unverified; the designed waveform, which is obtained by SDP and the rank of $\mathbf{P}^*$ to the optimization problem 5.40 is equal to 1 or which is obtained by SDP plus a randomized algorithm, is called Waveform SDP; the designed waveform, which is obtained by an iterative algorithm, is called Waveform by Iterative Algorithm.

If $T_I \to 0$, which means the integrator only captures one sample after ADC as the decision statistic, then spectral mask, notch line of Arbitrary Notch Filter, the designed waveforms and multipath impulse response represented in the frequency domain are shown in Figure 5.4. Meanwhile, the designed waveforms in time domain are shown
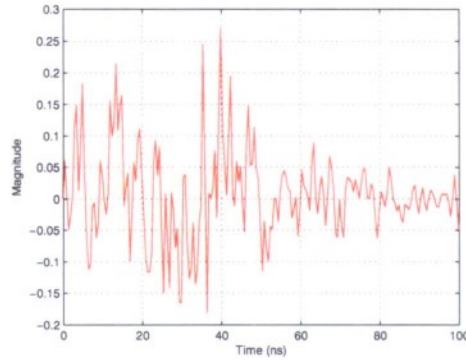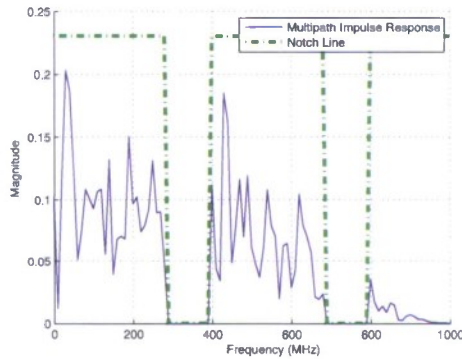
Figure 5.2: Multhpath impulse response.

Figure 5.3: Multipath impulse response and notch line of Arbitrary Notch Filter represented in the frequency domain.

in Figure 5.5. Figure 5.6 shows the convolution between the designed waveforms and multipath channel impulse response. In this case spectral mask constraint is not tight. The peak value of noiseless signal in Figure 5.6 is 1. If the arbitrary spectral mask constraint is imposed on the transmitted waveform, then spectral mask, notch line of Arbitrary Notch Filter, the designed waveforms and multipath impulse response represented in the frequency domain are shown in Figure 5.7. Meanwhile, the designed waveforms in time domain are shown in Figure 5.8. Figure 5.9 shows the convolution between the designed waveforms and multipath channel impulse response. The peak value of the noiseless signal in Figure 5.9 is 0.94. This sharp peak can give us benefits for wireless communication.

In sum, when $T_I \to 0$, the waveform by an iterative algorithm is the same as the waveform by SDP. SDP always gives the optimal solution to the optimization problem 5.35, which means the rank of $\mathbf{P}^*$ to the optimization problem 5.40 is always equal to 1. The reason of this result is that in this kind of situation the rank of $\mathbf{H}_o$ is equal to 1. Meanwhile, the transmitted waveform satisfies the spectral mask constraint, which will make cognitive radio have no interference to primary radio. Besides, cognitive radio will transmit the waveform such that the energy will not be transmitted in the notched frequency band at the receiver in order to save the energy. Thus, the designed waveform can be treated as a wideband non-continuity signal.

If T_I is equal to $20ns$, then two different spectral masks are considered. One spectral mask and the corresponding notch line of Arbitrary Notch Filter, the designed waveforms and multipath impulse response represented in the frequency domain are shown in Figure 5.10. The other is shown in Figure 5.11. When T_I is larger than 0, only SDP
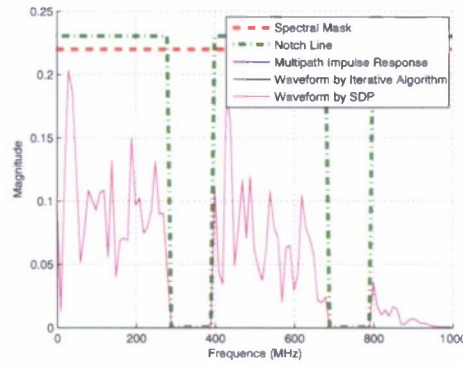
Figure 5.4: Spectral mask, notch line of Arbitrary Notch Filter, the designed waveforms and multipath impulse response represented in the frequency domain when $T_I \to 0$.

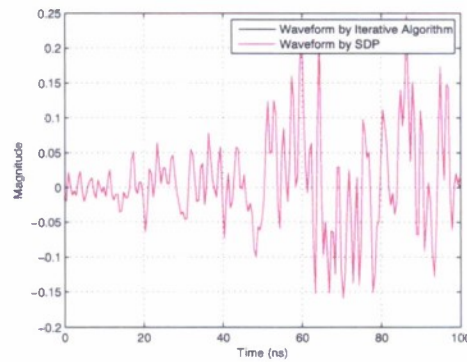Figure 5.5: Designed waveforms in the time domain when $T_I \to 0$.

can not guarantee the optimal solution at all times because the rank of $\mathbf{P}^*$ to the optimization problem 5.40 can not be always equal to 1. In the first case, only SDP gives the optimal solution. But in the second case, the waveform obtained only by SDP violates the spectral mask constraint in some frequency points, and SDP plus a randomized algorithm gives the suboptimal solution.

5.5 Discussion

This chapter deals with wideband waveform optimization with energy detector in cognitive radio. Wideband waveform is designed according to the optimization objective with the considerations of the spectral mask constraint at the transmitter and the influence of Arbitrary Notch Filter at the receiver. The optimization problem is formulated as QCQP. After relaxation, QCQP can be solved by using SDP plus a randomized algorithm. Meanwhile, a computationally-efficient iterative method is proposed to give the optimal solution for a special situation where the integrator only captures one sample after ADC as the decision statistic.
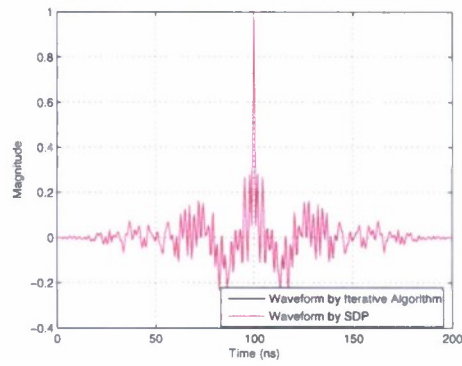
Figure 5.6: Convolution between the designed waveforms and the multipath impulse response when $T_I \to 0$.
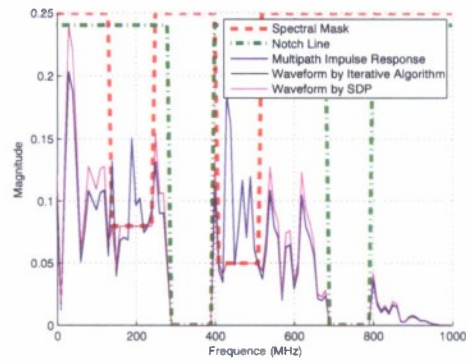

Figure 5.7: Spectral mask, notch line of Arbitrary Notch Filter, the designed waveforms and multipath impulse response represented in the frequency domain when $T_I \to 0$.
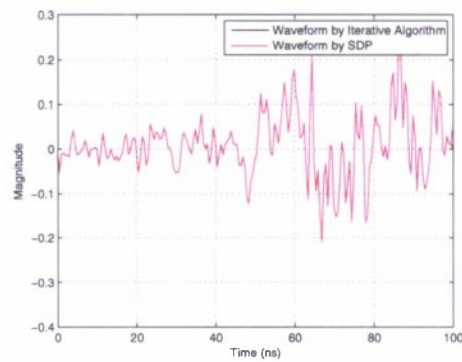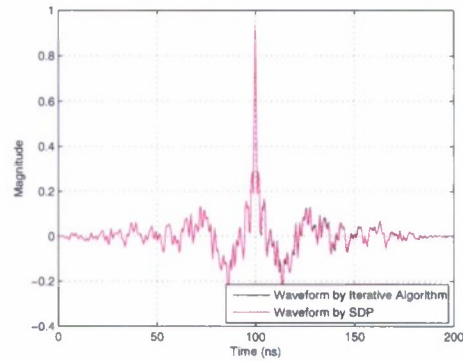

Figure 5.8: Designed waveforms in the time domain when $T_I \to 0$.

Figure 5.9: Convolution between the designed waveforms and the multipath impulse response when $T_I \to 0$.
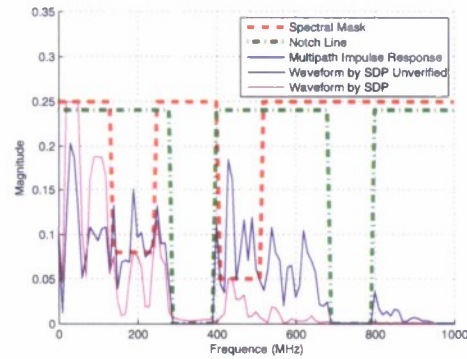

Figure 5.10: Spectral mask, notch line of Arbitrary Notch Filter, the designed waveforms and multipath impulse response represented in the frequency domain when T_I is $20ns$.
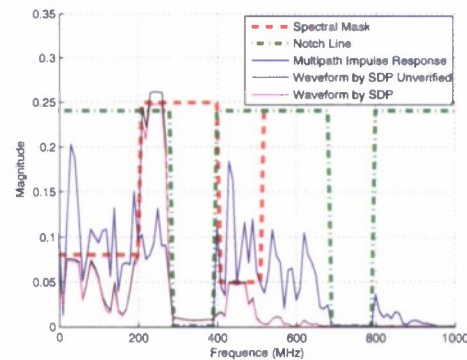

Figure 5.11: Spectral mask, notch line of Arbitrary Notch Filter, the designed waveforms and multipath impulse response represented in the frequency domain when T_I is $20ns$.

Bibliography

[1] D. Singh, Z. Hu, and R. C. Qiu, "UWB Channel Sounding and Channel Characteristics in Rectangular Metal Cavity," in *Proc of IEEE Southeastern Symposium*, 2008.

[2] R. C. Qiu, C. Zhou, J. Q. Zhang, and N. Guo, "Channel Reciprocity and Time-Reversed Propagation for Ultra-Wideband Communications," in *IEEE AP-S International Symposium on Antennas and Propagation*, 2007.

[3] N. Guo, Z. Hu, A. S. Saini, and R. C. Qiu, "Waveform-level Precoding with Simple Energy Detector Receiver for Wideband Communication," in *IEEE SSST'09*, 2009.

[4] *http://www.stanford.edu/ boyd/cvx/*.

[5] A. Man and C. So, "Improved approximation bound for quadratic optimization problems with orthogonality constraints," in *Proceedings of the Nineteenth Annual ACM-SIAM Symposium on Discrete Algorithms*, pp. 1201–1209, Society for Industrial and Applied Mathematics Philadelphia, PA, USA, 2009.

[6] A. Nemirovski, "Sums of random symmetric matrices and quadratic optimization under orthogonality constraints," *Mathematical Programming*, vol. 109, no. 2, pp. 283–317, 2007.